Chemistry, Physics and Technology of Surface. 2024. V. 15. N 4. P. 561-573

UDC 544.723:546.791.6 doi: 10.15407/hftp15.04.561

O.V. Perlova [1], Yu.S. Dzyazko [2], M.E. Karimova [1], O.V. Palchik [2], L.M. Ponomaryova [3], E.O. Kolomiiets [2]

MAGNETITE-CONTAINING COMPOSITE BASED ON CORN COB CELLULOSE FOR ADSORPTION OF U(VI) COMPOUNDS

[1] Odesa I.I. Mechnikov National University
2 Dvoryanska Str., Odesa, 65082, Ukraine, E-mail: olga_perlova@onu.edu.ua
[2] V.I. Vernadskii Institute of General and Inorganic Chemistry of National Academy of Sciences of Ukraine
32/34 Acad. Palladin Ave., Kyiv, 03142, Ukraine
[3] Sumy State University
116 Kharkivska Str., Sumy, 40000, Ukraine

Sources of U(VI) compounds in ground and surface water are uranium-containing minerals and anthropogenic activity: nuclear and thermal power plants, mineral processing plants, mines, testing nuclear weapon. Due to toxicity and radioactivity of the compounds of this metal, their content in water is strictly regulated. In order to remove small amount of U(VI) from water, adsorption and ion exchange look most attractively. In this work, magnetite-containing composite adsorbent based on cellulose, which was produced from corn cobs, has been developed. Its advantages over synthetic adsorbents are cheap and available feedstock as well as a simple manufacture procedure. In order to provide high magnetite content (≈ 13.5 mass. %), both hydrophilic and hydrophobic constituents were removed from cellulose before the particle embedding. Mesopores, a size of which are 10 nm, make a contribution to porous structure of the composite and magnetite, pure cellulose is characterized by microporous structure. Comparing with this material, the composite shows a wider pH interval of U(VI) adsorption. The most favorable conditions are realized at pH 4–6, when the degree of uranium removal reaches 87–97 %. The composite shows a synergetic effect demonstrating the fastest adsorption than both magnetite and cellulose. Moreover, higher capacity of adsorption monolayer was found for the composite (0.71 mmol g^{-1}) comparing with magnetite (0.14 mmol g^{-1}). For utilization, the adsorbent can be added to uranium-containing ore before its treatment.

***Keywords**: uranium adsorption, cellulose, corn cobs, magnetite, composite*

INTRODUCTION

Uranium is related to dispersed element, since its content in rocks is rather low (up to 0.003 mass. %) [1, 2], ocean and sea water contains lower U amount (about 3 ppb) [2, 3]. Such U-containing minerals as autunite, carnotite, monazite, samarskite, and uraninite or pitchblende are found in rocks with high silicon content (sands, sandstones and so on). Namely these minerals are a sources of U(VI) compounds in ground and surface water. They also appear in water as a result of anthropogenic activity: nuclear and thermal power plants, mineral processing plants, mines, testing nuclear weapon. Depleted uranium containing less than 0.3 % of radioactive ^{235}U isotope also produces U(VI) compounds [4, 5]. It is involved into the production of non-nuclear weapons: for instance, about ≈ 10 tons of depleted uranium were scattered in Kosovo due to projectiles containing this component [5–7]. Now the projectiles of this type are used in Ukraine.

The transformation of metallic uranium into oxidized U_3O_8 ($U_2O_5 \cdot UO_3$) form is enhanced under elevated temperatures and humidity, especially as a result of explosion [8, 9]. When U_3O_8 is hydrated and further oxidized in soil and water so generating UO_2^{2+} complexes with chloride, sulphate, carbonate and nitrate anions. Analogically to other heavy metal ions, UO_2^{2+} cations demonstrate high chemical toxicity, since they form bonds with proteins via carboxyl [10], amino- [11] and sulfide [12] groups. They are attached to the cell membrane with these irreversible binding and violate its functions and also the functions of ferments and cells [13]. Thus, the negative impact of UO_2^{2+} ions on the soil [14] and aquatic [15] ecosystems has been confirmed. These species can entry to the human organisms through food chains [16] or directly with drinking water [17] causing diseases of kidney, liver, heart and other organs [9, 18].

Due to the negative impact on human health, the maximal allowable concentration of

U(VI) in drinking water is 20 μg dm^{-3} according to the US Environmental Protection Agency [19]. Regarding industrial wastewater, containing high amount of U(VI) compounds, flotoextraction technique can be recommended [20]. In order to reach the maximal allowable concentration, adsorption or ion exchange techniques are desirable. Among synthetic materials for this purpose, ion exchange fibers [21], polymer-inorganic ion exchange resins [22], ferrocyanides [23] and advanced carbon nanomaterials [24], such as functionalized carbon nanotubes [25, 26], oxidized graphene [27, 28] or graphene aerogel [29] should be mentioned. The problem of finely dispersive adsorbents, such as carbon nanomaterials or ferrocyanides of heavy metals, they are framed with oxides of multivalent metals [30–32], polymers [33, 34] or microorganisms [35].

It should be stressed that the oxides of multivalent metals occupy special position among known sorption materials, since they possess amphoteric properties: depending on the solution pH, cation or anion exchange ability dominates [36, 37]. This property is favourable for U(VI) sorption, since this metal can exist both in cationic and anionic forms in aqueous media [38, 39]. It is possible to control the surface charge of oxides by the variation of their chemical composition [40, 41]. This approach allows one to regulate sorption of ions of one or other charge [42, 43]. Other advantage of oxides is no sufficient deviation of the solution pH from the initial value, since sorption of the U(VI) compounds is strongly affected by the solution acidity [30–32, 44–46]. Among known oxide materials, magnetite is favorable for U(VI) sorption due to fast sorption rate [47, 48] and the negligible effect of ionic strength [48]. For instance, the equilibrium time is much shorter than 24 h at pH 7, when the initial concentration of U(VI) species is 0.1–0.2 mol dm^{-3} [47]. The equilibrium time of 6 h is reported in [48]. In this case, the U(VI) concentration was 0.85–0.13 mmol dm^{-3}. When the sorbent dosage is 1 g dm^{-3}, the capacity of 25 μmol g^{-1} is reached at pH 7. Insufficient effect of ionic strength was also noted: when this parameter is 0.025–0.2 mol dm^{-3}, the capacity is 20 and 18 μmol g^{-1}. No influence of ionic strength on U(VI) sorption within the interval of 0.001–0.2 mol dm^{-3} (pH 5.5–8.5) is also noted in [49], this is explained by the surface complexation. Other explanation is partial U(VI)→U(IV) reduction, when such oxides as UO_2 [47, 50], U_3O_8 and UO_3 are formed [47].

Insufficient effect of ionic strength is caused by partial U(VI)→U(IV) reduction [49] and surface complexation [50]. Other advantage of magnetic particles is a possibility to separate nanoparticles with a magnet, *i.e.* without filtration or centrifugation. However, adsorption active magnetite can be obtained in a form of finely dispersive powder. It means the difficultness of its removal from liquids despite magnetic properties. To avoid this problem, they are coupled with a coarse component, which also adsorbs U(VI) compounds. These components are coarse flakes of oxidized graphene [51], graphene with MOF [52] *etc*.

Among the matrices, into which magnetic particles could be embedded, non-carbonized natural cellulose-based adsorbents look rather promising, since they are able to adsorb heavy metal ions [53]: Pb^{2+} [54–60], Cu^{2+} [55, 57, 59], Cd^{2+} [56, 57, 59, 60]. Other advantages are availability and various plant feedstock, such as sago [54], fern [55], mango peels [56], olive pomace [57], maize bran [58], sugarcane bagasse [59] and corn cobs [60], was used for the sorbent preparation. Agricultural wastes can be also applied to the sorption removal of U(VI) compounds from water. Sorption materials can be obtained from aloe [61], date stones [62], pomegranate peels [63], rice stems [64], eichhornia crassipes [65], tea leaves [66], solanum incanum [67], lemon [68] and red beet peels [69], sugarbeet pulp [70].

As found previously, corncob-based composites are characterized by considerable adsorption capacity towards heavy metal ions (up to 0.25 mmol g^{-1}) [60]. Though the capacity is lower comparing with synthetic materials, this disadvantage is compensated by availability of feedstock for the adsorbent production. The aim of this work is to evaluate the performance of this composite towards U(VI) removal from water.

EXPERIMENTAL

A feedstock for the adsorbent preparation was corn cobs (*Zea mays*). The raw material was crushed, washed with water, dried under ambient conditions down to a constant mass, and treated with 10 % NaOH solution for 24 h to remove hydrophilic inclusions like pectins and hemicellulose. Then the material was rinsed with

water, dried at room temperature and rinsed with petrol. This approach allowed us to remove hydrophobic inclusions, such as lignin and wax, and to exclude good flotation as opposed to [60]. After the treatment with petrol, the samples were dried under ambient conditions and then at 120 °C. Plant cellulose was obtained by this manner.

A weighted sample of the cellulose was modified with magnetite according to the method [71] similarly to [60]. The sample was impregnated with water under vacuum, then with a mixed solution containing $FeCl_2$ (0.1 M) and $FeCl_3$ (0.2 M). A 10 M NH_4OH solution was added drop by drop under agitation up to pH 11. Magnetite was formed as a result of reaction:

$$FeCl_2 + 2FeCl_3 + 8NH_4OH \rightarrow$$

$$\rightarrow Fe_3O_4 + 8NH_4Cl + 4H_2O. \quad (1)$$

The composite was rinsed with water and down to pH 7, dried under ambient conditions and at 120 °C. The magnetite powder, which was precipitated outside cellulose, was collected for investigations.

For SEM observation and recording energy dispersive spectra, a SEO-SEM Inspect S50-B microscope (FEI Company, USA) was used. The samples were preliminarily coated with ultrathin Ag film. Porous structure at the level of micropores and mesopores was investigated with a Quantachrome Autosorb 6B device (Quantachrome instruments).

A size of particles (d) was determined using sieves with holes of different diameter (40 μm – 3 mm). A contribution of each fractions (ω) was determined via:

$$\omega = \frac{m_f}{m_t} \times 100\% \quad (2)$$

where m_f and m_t are the mass of fraction and total mass of adsorbent respectively. The average size of particles (d) in each fraction was estimated as:

$$d = \sqrt[3]{\frac{2d_1^2 d_2^2}{d_1 + d_2}} \quad (3)$$

where d_1 and d_2 are the diameters of holes of adjacent sieves.

A pH of the point of zero charge (PZC) was determined similarly to [72]. A series of a 0.05 M KCl solutions (40 см^3 of each) was prepared, their pH was regulated with 0.1 M HCl or KOH solutions. Then the liquid volume was increased up to 50 см^3 with a KCl solution, 0.1 g of adsorbent was added. The flasks were shacked intensively with a Water Bath Shaker Type 357 system (Elpan, Poland) during 48 h, then the pH was measured using a with a I–160 MI pH-meter (Analitprylad, Ukraine). The differences between the initial and final pH was determined for each solution, then obtained values were plotted vs initial pH. The PZC corresponded to the intersection of the curve with abscissa axis.

Adsorption of U(VI) was investigated under batch conditions, a system of solution-adsorbent was vigorously shacked. The ratio of the masses of solid and liquid was 1:500, the temperature was kept at 20±1 °C. To study the adsorption rate, a weighted sample of the adsorbent (0.05 g) was in contact with the solution (25 cm^3) containing 2.1×10^{-4} mol dm^{-3} of U(VI) (50 mg dm^{-3}), the initial pH of the solution was 6. The contact time was 5–120 min. Samples (2 cm^3) were periodically taken, filtered through the filter with pores of 13–25 μm and analyzed later.

The effect of pH was researched as follows. A pH of the solution containing 2.1×10^{-4} mol dm^{-3} of U(VI) was regulated with 0.1 M HCl or KOH solutions in the interval of 2–8. Then the weighted samples of adsorbent were added. The contact time was 48 h.

When the adsorption isotherms were investigated, the concentration interval was 2.1×10^{-5}–2.1×10^{-4} mol dm^{-3}, the initial pH was 6.

The solution after adsorption was analyzed according to the method [73]. An aliquot of the filtrate (2 cm^3) was diluted up to 10 cm^3, 10 % hexamine solution was added to achieve the pH of 5.5, then 1 cm^3 of 0.1 % Arsenazo III solution was put on the solution. The solution was diluted to 25 cm^3 with deionized water. The absorbance was measured at 640 nm by means of a Shimadzu UV-mini1240 spectrophotometer (Shimadzu, Japan).

A degree of U(VI) removal from the solution (R) and sorption capacity (A) were calculated via:

$$R_s = \frac{C_i - C}{C_i} \times 100\% \quad (4)$$

$$A = \frac{V_s(C_i - C)}{m}, \quad (5)$$

where C_i and C are the initial and equilibrium concentration respectively, V_S is the solution volume, m is the sorbent mass.

RESULTS AND DISCUSSION

Low-resolution SEM images allows us to observe the largest structure elements of plant cellulose, namely fiber bundles (Fig. 1 *a*). Their thickness are irregular (1–10 μm). The bundles are chaotically intertwined forming cellular structure with holes, a size of which is from several to several tens microns. Modifying causes partial destruction of the cellular structure (Fig. 1 *b*). The bundles show cracks, their width is from up to 1 μm. Moreover, large particles of irregular shape are visible on the surface, these fragments are probably related to the fragments of biopolymer. Additionally, small particles (≤ 1 μm), a shape of which is close to globular, are visible, their size is smaller than 1 μm.

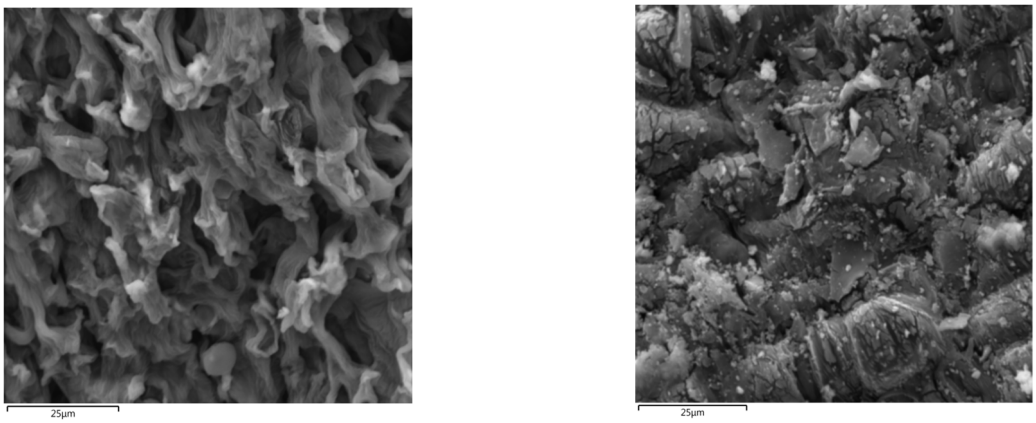

a *b*

Fig. 1. SEM images of pristine cellulose (*a*) and its magnetite-containing composite (*b*)

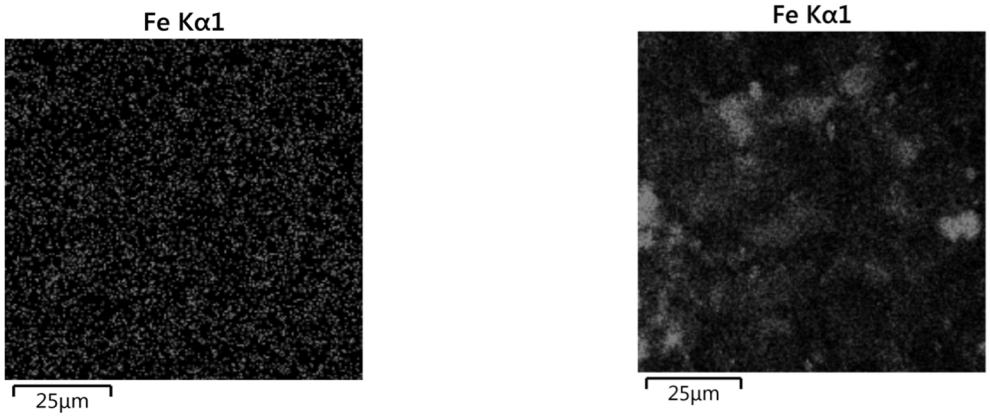

a *b*

Fig. 2. Maps of the Fe distributions in pristine (*a*) and modified cellulose (*b*)

According to elemental analysis, iron is homogeneously distributed through the matrix of cellulose that is free from both hydrophilic and hydrophobic components (Fig. 2 *a*). The content of this element in the biopolymer matrix was found to be 0.37 mass. %, it is typical for microelements (the energy dispersive spectrum is given in Fig. 3 *a*). For comparison, the amount of Cu is 0.74 %.

It should be also stressed, that the content of Al is 0.2 %. In general, soil contains 0.03 % of Al in a form of mobile compounds. It means the capability of corn to accumulate this element. The energy dispersive spectrum shows a presence of Si, however, its content is lower than 0.1 %. This element penetrates into plant in a form of soluble metasilicates, which are formed from insoluble silicates under the influence of microorganisms.

The map of Fe distribution in the composite shows higher concentration of this element in the biopolymer matrix (see Fig. 2 *b*). Its distribution is more heterogeneous, the regions of elevated Fe content are visible as opposite to unmodified cellulose. The concentration of this metal is 9.74 % (the energy dispersive spectrum is shown in Fig. 3 *b*). It means the content of magnetite is 13.45 %. Let us make some quantitative estimations. Bulk density (determined with Archimedes method) and apparent density (estimated from the mass of sample and its geometrical parameters) of corn cellulose is 1.5 and 0.3 g cm^{-3} respectively. It means that 1 g of biopolymer contains 1.95 cm^3 of pores which can be filled with a solution of Fe(II) and Fe(III) during the modifying procedure. Thus, 0.22 g of magnetite can be deposited from this volume of solution taking into consideration the concentration of iron salts. Thus, 1 g of the composite can contain 18 % of magnetite and even larger, since some amount of the modifier is deposited on the outer surface. Nevertheless, smaller amount of magnetite has been found evidently due to closed pores of the cellulose, which are unavailable for liquids.

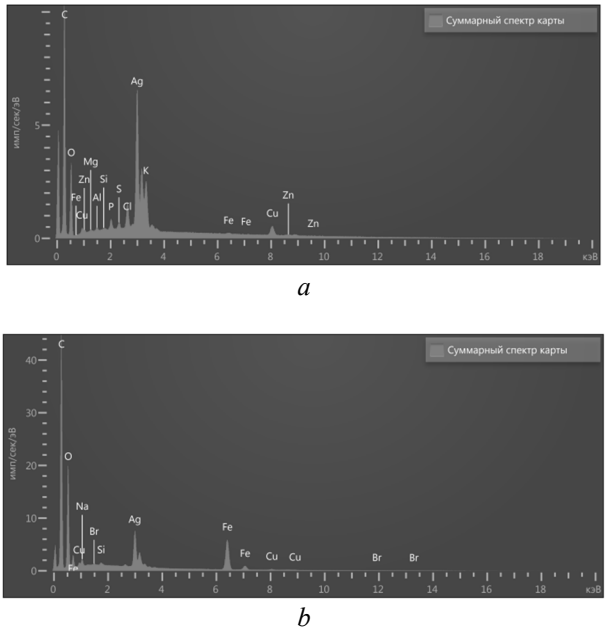

a

b

Fig. 3. Energy dispersive spectra for cellulose after the removal of hydrofilic and hydrophobic components (*a*), and magnetite-containing composites (*b*)

Fe-based adsorbent was related to magnetite according to the XRD analysis, the pattern was given earlier [60]. Among investigated adsorbents, the inorganic material is characterized by the smallest particle size: the fraction of micron size dominates (Table 1). The particle size of the adsorbent produced from corn cobs depends on grinding. In our case, the adsorbent contains mainly large particles, the maximal size of which is about 2 mm. Namely this fraction dominates.

Table 1. Characterization of the samples

Parameter	Magnetite	Cellulose	Composite
Particle size, mm	0.056–0.464	0.198–2.735	0.198–2.735
Size of dominated particles, mm	0.056	1.916	1.916
pH PZC	6.3	4.1	4.1
Size of dominating pores, nm	<1	10	10
Surface area, $cm^3\ g^{-1}$	140	1.5	20
Volume of micro- and mesopores, $cm^3\ g^{-1}$	0.414	0.006	0.058

The sufficient advantage of magnetite over biopolymer is much higher surface area and also larger volume of micro- and mesopores, which determine the selectivity and rate of adsorption. A size of dominating pores is 10 nm (Fig. 4). The pore size distribution shows also a shoulder, which corresponds to 2–4 nm. The maximum is located in a wide region (1–20 nm) indicating irregular pores due to widenings-narrowings as well as tortuosity. Biopolymer demonstrates a fragment of sharp peak at < 2 nm. A diffuse maximum is located at 2.5 nm. Regarding the composite, the peak position coincides with that for magnetite, however, the maximum is rather diffuse. It is possible to suggest that the inorganic constituent determines porous structure of the composite. Their specific surface area and volume of small pores are the values of the same order.

As opposite to porous structure, namely biopolymer affects the pH of PZC: in the case of biopolymer and cellulose these magnitudes are similar. Positive charge of the cellulose surface is due to adsorption of H^+ ions, the negative charge is caused by dissociated carboxyl groups and also by OH^- adsorption (carboxyl groups were recognized earlier [60]). Regarding magnetite, the pH of PZC is higher and close to neutral. Positive or negative charge is due to protonation or dissociation of hydroxyl groups respectively, adsorption of H^+ or OH^- ions can also make their contribution. Charge surface determines adsorption of uranium species on magnetite, cellulose and their composite.

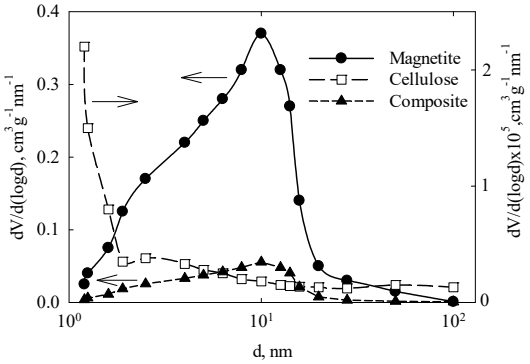

Fig. 4. Pore size distributions for polymer, inorganic and polymer-inorganic adsorbents

Other sufficient factor, which affects U(VI) adsorption is its speciation in a solution. Regarding chloride-containing media, UO_2^{2+} cations dominate at pH 2–4 [74]. However, the surface of adsorbents is charged positively, that is why adsorption of U(VI) at pH 2 is inconsiderable (Fig. 5). Adsorption is enhanced within the order: cellulose<composite<magnetite. In this case, U(VI) complexation with carboxyl (cellulose, composite) and hydroxyl groups (magnetite) as well as U(VI) reduction (magnetite, composite) play a key role.

At pH 4–4.5, both $UO_2(OH)^+$ and UO_2^{2+} cations coexist in a solution. In this case, the removal degree exceeds 70 %. Maximal adsorption is achieved at 4.5 (cellulose) and 4 (composite). Regarding magnetite, the removal degree shows a plateau in a wide pH interval (4–10) with a tendency to decrease in alkaline media. A plateau is evidently caused by the U(VI)→U(IV) transformation.

A decrease of adsorption is at pH > 4–4.5 (cellulose, composite) is due to the appearance of uncharged $UO_2(OH)_2$ species, which is in colloidal form. Moreover, $UO_2(OH)_3^-$ anions exist at pH > 6. In this region, physical adsorption on cellulose is possible. In the case of composite, adsorption can be accompanied by the U(VI) reduction. It should be stressed that the maximum of the R – pH for the composite is much wider comparing with cellulose.

The rate of U(VI) adsorption is shown in Fig. 6 *a*. The $R - t$ curves (where t is the time) show the regions of fast growth and plateau. The equilibrium is reached after 15 (composite) and 20 (magnetite and cellulose) min. of the contact of a solution with adsorbent. At the same time, the highest removal degree (97 %) is reached for the composite. Magnetite demonstrates lower R value (94 %), the lowest magnitude has been found in the case of cellulose (80 %).

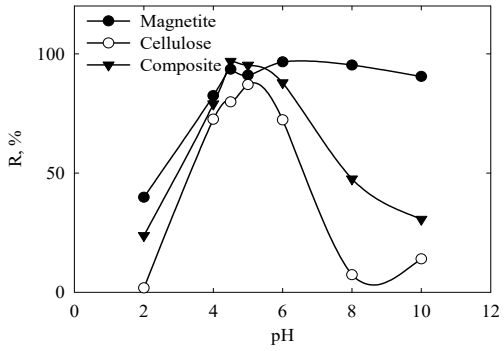

Fig. 5. Effect of pH on U(VI) adsorption

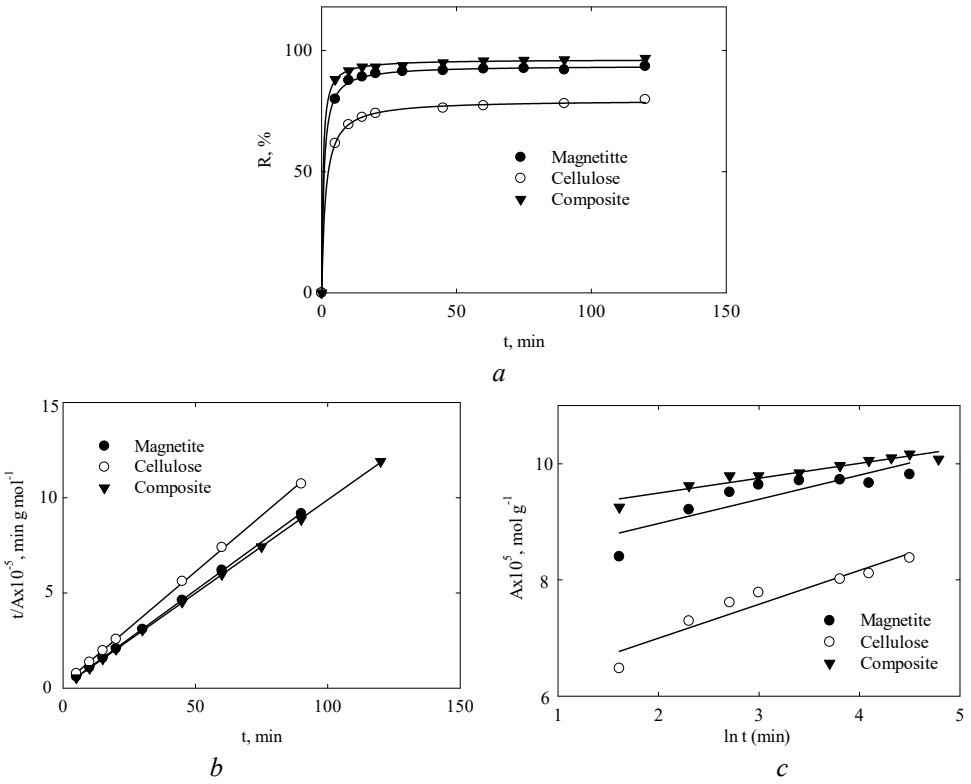

Fig. 6. Degree of U(VI) removal as a function of time (*a*), application of the model of pseudo-second order (*b*) and Elovich model (*c*)

The model of chemical reaction of pseudo-second order proposed by Ho and McKay was applied (Fig. 6 *b*) [75, 76]:

$$\frac{\mathrm{t}}{\mathrm{A}} = \frac{1}{\mathrm{KA}_{\infty}^{2}} + \frac{1}{\mathrm{A}_{\infty}} \cdot \mathrm{t}, \qquad (6)$$

where K is the rate constants, A_∞ is the equilibrium adsorption capacity. As seen from Fig. 6 *b*, the t/A – t curves are linear. The model parameters are given in Table 2. Very high values of the correlation coefficient are observed for all three sorbents. Moreover, the experimental and model A_∞ magnitudes are very close to each other. The highest initial adsorption rate (r_0):

$$r_0 = KA_{\infty}^{2} \qquad (7)$$

was found for the composite. According to the model, cellulose shows the slowest adsorption rate, the fastest rate is attributed to composite. This can be explained by higher reactive ability of adsorption centres of embedded magnetite for U(VI) species. However, the constants of equ. (6)

are practically the same for both materials. Pseudo-order is due to a small concentration of adsorbed ions comparing with the concentration of adsorption centres.

The Elovich model can be also applied to describe the adsorption rate [77]. This equation is often used for describing chemisorption in heterogeneous systems, when the rate decreases exponentially with increase of adsorption capacity. The interaction between adsorbed ions is also suggested. The model takes into consideration both adsorption and desorption:

$$A = \frac{1}{\beta} ln(\alpha\beta) + \frac{1}{\beta} \ln t . \quad (8)$$

Here α is the initial adsorption rate, β is the constant of the desorption rate. The results are given in Table 3. Rather low correlation coefficient is due to scattering data. Nevertheless, the *A*-ln*t* curves can be linearized demonstrating a tendency of increasing adsorption capacity over time. The highest initial adsorption rate and desorption constant have been found for the composite. Cellulose shows the lowest values. Magnetite occupies an intermediate value. Regarding the regularities of adsorption rate, the data for cellulose and composite are in agreement with the model of pseudo-second order. Chemisorption means complexation of U(VI)-containing ions with carboxyl (cellulose, composite) or hydroxyl groups (magnetite, composite).

Table 2. Application of the model of pseudo-second order to U(VI) adsorption

Adsorbent	$A_\infty \times 10^5$, mol g^{-1}		Correlation coefficient	$K \times 10^3$, g mol^{-1}min^{-1}	$r_0 \times 10^4$, mol g^{-1}min^{-1}
	Experimental	Model			
Magnetite	9.8	9.9	0.9999	15.0	1.45
Cellulose	8.4	8.5	0.9996	6.4	0.45
Composite	10.1	10.2	0.9999	15.1	1.53

Table 3. Application of the Elovich model to U(VI) adsorption

Adsorbent	$\beta \times 10^{-5}$, dm^3 mol^{-1}	α, mol g^{-1}min^{-1}	Correlation
Magnetite	2.5	1.94×10^3	0.7404
Cellulose	1.7	0.11	0.9169
Composite	3.3	3.21×10^7	0.9479

The dependences of U(VI) removal degree on the initial solution concentration are given in Fig. 7 *a*. The *R* value predictably decreases within the interval of 2.1×10^{-5}–2.1×10^{-4} mol·dm^{-3}. However, a decrease of the removal degree is not too sufficient (8–17 %). The curves show wide plateau in a wide interval of concentration.

Isotherms (dependences of adsorption capacity on the equilibrium concentration of the solution) are given in Fig. 7 *b*. They show 2 semi-waves in the case of magnetite and composite. Regarding cellulose, the isotherm is characterized by sigmoidal shape.

As found, the Langmuir approach [77] was found to be the most adequate to describe the curves. This model allows us to obtain linear dependencies with high correlation coefficient on the one hand and to evaluate reliable constants on the other hand. Following equation was used:

$$\frac{1}{A} = \frac{1}{K_L A_{ml} C} + \frac{1}{A_{ml}}, \quad (9)$$

where A_{ml} is the monolayer capacity, the K_L parameter characterizes energy of interaction of molecules with surface. The data are given in Table 4. As shown, much higher monolayer capacity was found for the composite comparing with magnetite. At the same time, the K_L constant is smaller for the composite indicating lower interaction of U(VI) with surface.

The Dubinin-Radushkevich model [77]:

$$ln A = ln A_{DR} - \frac{R^2 T^2}{E^2} \left[ln(1 + 1/C) \right]^2 \quad (10)$$

was found to be the most suitable to fit the adsorption isotherm for cellulose ting linear approximation within a certain interval of concentration of equilibrium solution (Fig. 7 *d*). Here A_{DR} is the Dubinin-Radushkevich constant, which is related to total capacity, E is the adsorption energy (Table 4). The energy value is in the interval of 8-16 kJ mol^{-1} indicating ion exchange mechanism of adsorption. The application of this model shows that large UO_2^{2+} ions occupy whole volume of micropores. Indeed, microporosity follows from the pore size distribution (see Fig. 4). Based on the obtained results, faster adsorption of U(VI) on the composite comparing with cellulose can be explained by screening biopolymer pores with inorganic constituent similarly to [78], where the embedded particles of hydrated iron oxide accelerated sorption of Pb^{2+} ions.

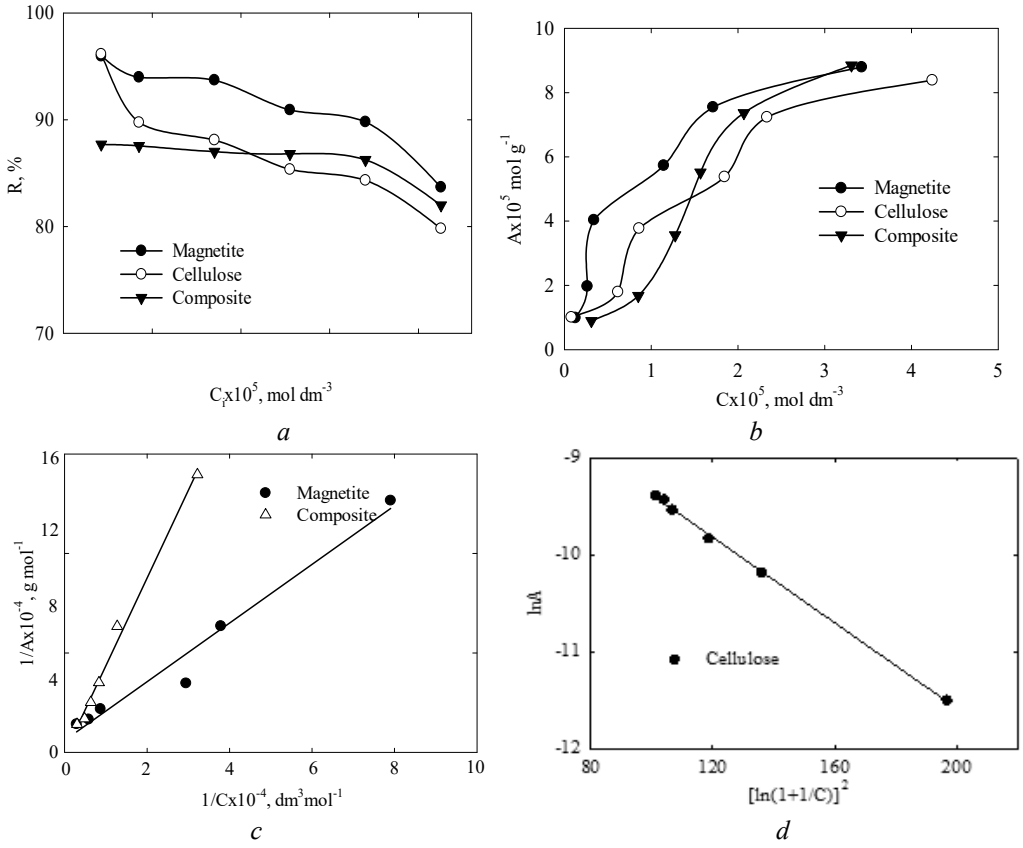

Fig. 7. Removal degree of U(VI) compounds *vs* their initial concentration (*a*), adsorption isotherms (*b*), application of Langmuir (*c*) and Dubinin-Radushkevich (*d*) models to adsorption on magnetite, composite (*c*) and cellulose (*d*)

Table 4. Application of Langmuir and Dubinin-Radushkevich model to adsorption isotherms

Adsorbent	$A_{ml}\times10^4$, mol g^{-1}	$K_L\times10^{-4}$, dm^3 mol^{-1}	$A_{DR}\times10^4$, mol g^{-1}	E, kJ mol^{-1}	Correlation
Magnetite	1.45	5.82			0.9995
Cellulose			8.3	11.37	0.9932
Composite	7.08	0.40			0.9924

CONCLUSIONS

Removal of hydrophobic components from the corn cob cellulose allows us to incorporate considerable amount of magnetite comparing with [60]. It means no flotation of the adsorbent particles in aqueous media giving a possibility to use the composite as an adsorbent. Comparing with corn cob cellulose, the magnetite-containing composite shows a wider pH interval of U(VI)

adsorption. The most favorable conditions are realized at pH 4–6, when the degree of uranium removal reaches 87–97 %. The composite shows a synergetic effect demonstrating the fastest adsorption than both magnetite and cellulose. Moreover, higher capacity of adsorption monolayer was found for the composite comparing with magnetite. The adsorbent loaded with U(VI) can be added to uranium ore for further recovery of this metal.

The advantage of composite over pure inorganic constituent is coarse dispersion, this facilitates the separation of adsorbent from liquids. The advantages over synthetic adsorbents are cheap and available feedstock as well as a simple manufacture procedure.

Магнетитовмісний композит на основі целюлози качанів кукурудзи для адсорбції сполук U(VI)

О.В. Перлова, Ю.С. Дзязько, М.Е. Карімова, О.В. Пальчик, Л.М. Пономарьова, Є.О. Коломієць

Одеський національний університет імені І.І. Мечникова
вул. Дворянська, 2, Одеса, 65082, Україна, olga_perlova@onu.edu.ua
Інститут загальної та неорганічної хімії ім. В.І. Вернадського Національної академії наук України
пр. Академіка Палладіна, 32/34, Київ, 03142, Україна
Сумський державний університет
вул. Харківська, 116, Суми, 40000, Україна

Джерелами сполук U(VI) у підземних і поверхневих водах є урановмісні мінерали та антропогенна діяльність: атомні та теплові електростанції, збагачувальні комбінати, шахти, випробування ядерної зброї. Через токсичність і радіоактивність сполук цього металу, їхній вміст у воді суворо регламентується. Для видалення невеликої кількості U(VI) з води найбільш доцільними є методи адсорбції та іонного обміну. У даній роботі розроблено магнетитовмісний композиційний адсорбент на основі целюлози, отриманої з качанів кукурудзи. Переваги композиту перед синтетичними адсорбентами полягають у дешевій і доступній сировині для його виробництва, а також у простій процедурі синтезу. Щоб забезпечити високий вміст магнетиту (≈ 13.5 мас. %), перед модифікуванням із целюлози були видалені гідрофільні та гідрофобні складові. Пориста структура композиту та магнетиту формується, зокрема, мезопорами розміром 10 нм, а чиста целюлоза характеризується мікропористою структурою. Порівняно з цим матеріалом, композит демонструє ширший інтервал pH адсорбції сполук U(VI). Найбільш сприятливі умови реалізуються при pH 4–6, коли ступінь видалення урану досягає 87–97 %. Для композиту притаманним є синергетичний ефект: він демонструє найшвидшу адсорбцію, ніж магнетит і целюлоза. Крім того, виявлено вищу ємність адсорбційного моношару для композиту (0.71 ммоль $г^{-1}$) порівняно з магнетитом (0.14 ммоль $г^{-1}$). Для утилізації адсорбент можна додавати в урановмісну руду перед її обробкою.

***Ключові слова**: адсорбція урану, целюлоза, качани кукурудзи, магнетит, композит*

REFERENCES

1. Su X., Liu X., Du Z., Hou C., Li M., Cao F., Chen M., Zhang T. Advances in development of safe and efficient mining of coexisting coal and uranium resources. *Processes.* 2024. **12**(7): 1340.
2. Harmsen K., Haan F.A.M. Occurance and behaviour of uranium and thorium in soil and water. *Wageningen J. Life Sci.* 1980. **28**(1): 40.
3. Ku T.L., Mathieu G.G., Knauss K.G. Uranium in open ocean: concentration and isotopic composition. *Deep Sea Res.* 1977. **24**(11): 1005.
4. Bleise A., Danesi P.R., Burkart W. Properties, use and health effects of depleted uranium (DU): a general overview. *J. Environ. Radioact*. 2003. **64**(2–3): 93.
5. Ran Y., Wang S., Zhao Y., Li J., Ran X., Hao Y. A review of biological effects and treatments of inhaled depleted uranium aerosol. *J. Environ. Radioact*. 2020. **222**: 106357.

6. Pöllänen R., Ikäheimonen T.K., Klemola S., Vartti V.-P., Vesterbacka K., Ristonmaa S., Honkamaa T., Sipilä P., Jokelainen I., Kosunen A., Zilliacus R., Kettunen M., Hokkanen M. Characterisation of projectiles composed of depleted uranium. *J. Environ. Radioact.* 2003. **64**(2–3): 133.
7. Papastefanou C. Depleted uranium in military conflicts and the impact on the environment. *Health Phys*. 2002. **83**(2): 155.
8. Tamasi A.L., Boland K.**S.**, Czerwinski K., Ellis J.K., Kozimor S.A., Martin R.L., Pugmire A.L., Reilly D., Scott B.L., Sutton A.D., Wagner G.L., Walensky J.R., Wilkerson M.P. Oxidation and Hydration of U_3O_8 materials following controlled exposure to temperature and humidity. *Anal. Chem*. 2015. **87**(8): 4210.
9. Katz S.A. The chemistry and toxicology of depleted uranium. *Toxics.* 2014. **2**(1): 50.
10. Paranthaman S., Kubicki J.D., Guégan J.P., Châtellier X. Complexation of carboxyl groups in bacterial lipopolysaccharides: Interactions of H^+, Mg^{2+}, Ca^{2+}, Cd^{2+}, and UO_2^{2+} with Kdo and galacturonate molecules via quantum mechanical calculations and NMR spectroscopy. *Chem. Geol.* 2023. **273**(1–2): 55.
11. Kozai N., Ohnuki T. Association of uranyl ions with amino functional groups. *Chem. Lett*. 2009. **38**(2): 152.
12. Hu M.Z.C., Reeves M. Ligand-grafted biomaterials for adsorptive separations of uranium in solution. *AlChE J.* 1999. **45**(11): 2333.
13. Asic A., Kurtovic-Kozaric A., Besic L., Mehinovic L., Hasic A., Kozaric M., Hukic M., Marjanovic D. Chemical toxicity and radioactivity of depleted uranium: the evidence from in vivo and in vitro studies. *Environ. Res*. 2017. **156**: 665.
14. Gongalsky K.B. Impact of pollution caused by uranium production on soil macrofauna. *Environ. Monit. Assess.* 2003. **89**(2): 197.
15. Holdway D.A. Uranium mining in relation to impacts on inland waters. *Ecotoxicology*. 1992. **1**(2): 75.
16. Anke M., Seeber O., Müller R., Schäfer U., Zerull J. Uranium transfer in the food chain from soil to plants, animals and man. *Geochem*. 2009. **69**(2): 75.
17. Bjørklund G., Semenova Yu., Pivina L., Dadar M., Rahman M., Aasethi J. Uranium in drinking water: a public health threat. *Arch. Toxicol.* 2020. **94**: 1551.
18. Brine W. The toxicity of depleted uranium. *Int. J. Environ. Res. Public Health*. 2010. **7**(1): 303.
19. Hakonson-Hayes A.C., Fresquez P., Whicker F. Assessing potential risks from exposure to natural uranium in well water. *J. Environ. Radioact*. 2002. **59**(1): 29.
20. Perlova O.V., Shirykalova A.A. Flotoextraction removal of uranium(VI) using fine emulsified solutions of trialkylamine in white spirit. *J. Water Chem. Technol*. 2008. **30**(3): 385.
21. Perlova O.V., Tekmenzhi E.I., Perlova N.A., Polikarpov A.P. Dynamic sorption of carbonate forms of uranium (VI) with FIBAN fibrous ion exchangers. *Radiochem*. 2021. **63**(6): 762.
22. Perlova O., Dzyazko Yu., Halutska I., Perlova N., Palchik A. Anion exchange resin modified with nanoparticles of hydrated zirconium dioxide for sorption of soluble U(VI) compounds. In: *Nanooptics, Nanophotonics, Nanostructures, and Their Applications*. (Springer, 2018). P. 3.
23. Pshinko G.N., Puzyrnaya L.N., Yatsik B.P., Kosorukov A.A. Removal of U(VI) from aqueous media with layered double hydroxide of Zn and Al, intercalated with hexacyanoferrate(II) ions. *Radiochem*. 2015. **57**(6): 616.
24. Dzyazko Y., Perlova O., Martovyi I. Advanced carbon nanomaterials and their composites for removal of U(VI) compounds from aqueous solutions. In: *Nanooptics, Nanophotonics, Nanostructures, and Their Applications*. (Springer, 2023). P. 177.
25. Chen J.-H., Lu D.-Q., Chen B., OuYang P.-K. Removal of U(VI) from aqueous solutions by using MWCNTs and chitosan modified MWCNTs. *J. Radioanal. Nucl. Chem*. 2013. **295**: 2233.
26. Wu J., Tian K., Wang J. Adsorption of uranium (VI) by amidoxime modified multiwalled carbon nanotubes. *Prog. Nucl. Energy*. 2018. **106**: 79.
27. Yang P., Zhang H., Liu Q., Liu J., Chen R., Yu J., Hou J., Bai X., Wang J. Nano-sized architectural design of multi-activity graphene oxide (GO) by chemical post-decoration for efficient uranium(VI) extraction. *J. Hazard. Mater*. 2019. **375**: 320. https://doi.org/10.1016/j.jhazmat.2019.05.005.
28. Song W.C., Shao D.D., Lu S.S., Wang X.K. Simultaneous removal of uranium and humic acid by cyclodextrin modified graphene oxide nanosheets. *Sci. China Chem*. 2014. **57**(9): 1291.
29. Li N., Yang L., Wang D., Tang C., Deng W., Wang Z. High-capacity amidoxime-functionalized β-cyclodextrin/graphene aerogel for selective uranium capture. *Environ. Sci. Technol*. 2021. **55**(13): 9181.
30. Perlova O.V., Dzyazko Yu.S., Palchik O.V., Martovyi I.S. Hydrated titanium dioxide modified with potassium cobalt hexacyanoferrate (II) for sorption of cationic and anionic complexes of uranium(VI). *Appl. Nanosci.* 2022. **12**(4): 651.
31. Perlova O.V., Dzyazko Yu.S., Malinovska A.A., Palchik A.V. Peculiarities of U(VI) sorption on composites containing hydrated titanium dioxide and potassium-cobalt hexacyanoferrate(II). *Him. Fiz. Tehnol. Poverhni*. 2021. **12**(4): 344.
32. Perlova O.V., Ivanova I.S., Dzyazko Yu.S., Danilov M.O., Rusetskii I.A., Kolbasov G.Ya. Sorption of U(VI) compounds on inrganic composites containing partially unzipped multiwalled nanotubes. *Him. Fiz. Tekhnol. Poverhni*. 2021. **12**(1): 16.

33. Bai J., Chu J., Yin X., Wang J., Tian W., Huang Q., Jia Z., Wu X., Guo H., Qin Z. Synthesis of amidoximated polyacrylonitrile nanoparticle/graphene composite hydrogel for selective uranium sorption from saline lake brine. *Chem. Eng. J*. 2020. **391**: 123553.
34. Qian Y., Yuan Y., Wang H., Liu H., Zhang J., Shi S., Guo Z., Wang N. Highly efficient uranium adsorption by salicylaldoxime/polydopamine graphene oxide nanocomposites. *J. Mater. Chem. A.* 2018. **6**(48): 24676.
35. Zhao C., Liu J., Deng Y., Tian Y., Zhang G., Liao J., Yang J., Yang Y., Liu N., Sun Q. Uranium(VI) adsorption from aqueous solutions by microorganism-graphene oxide composites via an immobilization approach. *J. Cleaner Product*. 2019. **236**: 117624.
36. Wang L., Shi C., Pan L., Zhang X., Zou J.J. Rational design, synthesis, adsorption principles and applications of metal oxide adsorbents: a review. *Nanoscale*. 2020. **12**(8): 4790.
37. Al-Abadleh H.A., Grassian V.H. Oxide surfaces as environmental interfaces. *Surf. Sci. Rep.* 2003. **52**(3–4): 63.
38. Smedley P.L., Kinniburgh D.G. Uranium in natural waters and the environment: Distribution, speciation and impact. *Appl. Geochem.* 2023. **148**: 105534.
39. Aly M.M., Hamza M.F. A Review: Studies on Uranium Removal Using Different Techniques. Overview. *J. Dispers. Sci. Technol*. 2013. **34**(2): 182.
40. Mal'tseva T.V., Yatsenko T.V., Kudelko E.O., Belyakov V.N. The effect of introduction of manganese hydroxide and hydrated aluminum oxide on the pore structure and surface charge of Zr(IV), Ti(IV), and Sn(IV) oxyhydrates. *Russ. J. Appl. Chem*. 2011. **84**(5): 756.
41. Mal'tseva T., Pal'chik A., Kudelko E., Vasilyuk S., Kazdobin K. Impact of surface properties of hydrated compounds based on ZrO_2 on the value of ionic conduction. *J. Water Chem. Techol*. 2015. **37**(1): 18.
42. Kudelko E., Mal'tseva T., Belyakov V. Sorption of Cr(VI) ions by oxyhydrates of $M_xAl_{1-x}O_y \cdot nH_2O$ composition, where M is Zr(IV), Ti(IV), or Sn(IV). *Colloid J.* 2012. **74**(3): 313.
43. Maltseva T.V., Kudelko E.O., Belyakov V.N. Adsorption of Cu(II), Cd(II), Pb(II), Cr(VI) by double hydroxides on the basis of Al oxide and Zr, Sn, and Ti oxides. *Russ. J. Phys. Chem. A*. 2009. **83**(13): 2336.
44. Wang C.L., Li Y., Liu C.L. Sorption of uranium from aqueous solutions with graphene oxide. *J. Radioanal. Nuclear Chem*. 2015. **304**(3): 1017.
45. Akcay H. Aqueous speciation and pH effect on the sorption behavior of uranium by montmorillonite. *J. Radioanal. Nucl. Chem*. 1998. **237**: 133.
46. Zakutevskyy O.I., Psareva T.S., Strelko V.V. Sorption of U(VI) ions on sol-gel-synthesized amorphous spherically granulated titanium phosphates. *Russ. J. Appl. Chem*. 2012. **85**(9): 1366.
47. Missana T., Maffiotte C., García-Gutiérrez M. Surface reactions kinetics between nanocrystalline magnetite and uranyl. *J. Colloid. Interface Sci*. 2003. **261**(1): 154.
48. Das D., Sureshkumar M.K., Koley S., Mithal N., Pillai C.G.S. Sorption of uranium on magnetite nanoparticles. *J. Radioanal. Nucl. Chem*. 2010. **285**: 447.
49. El Aamrani S., Giménez J., Rovira M., Seco F., Grivé M., Bruno J., Duro L., de Pablo J. A spectroscopic study of uranium(VI) interaction with magnetite. *Appl. Surf. Sci.* 2007. **253**(21): 8794.
50. Missana T., García-Gutiérrez M., Fernańdez V. Uranium (VI) sorption on colloidal magnetite under anoxic environment: experimental study and surface complexation modelling. *Geochim. Cosmochim. Acta.* 2003. **67**(14): 2543.
51. El-Maghrabi H.H., Abdelmaged S.M., Nada A.A., Zahran F., El-Wahab S.A., Yahea D., Hussein G.M., Atrees M.S. Magnetic graphene based nanocomposite for uranium scavenging. *J. Hazard. Mater*. 2017. **322**: 370.
52. Amini A., Khajeh M., Oveisi A.R., Daliran S., Ghaffari-Moghaddam M., Delarami H.S. A porous multifunctional and magnetic layered graphene oxide/3D mesoporous MOF nanocomposite for rapid adsorption of uranium(VI) from aqueous solutions. *J. Ind. Eng. Chem*. 2021. **93**: 322.
53. Kolomiiets Y.O., Dzyazko Y.S. Sorbents based on non-carbonized vegetable raw materials. *Ukr. Chem. J*. 2022. **88**(5): 37.
54. Quek S.Y., Wase D.A.J., Forster C.F. The use of sago waste for the sorption of lead and copper. *Water SA*. 1998. **24**(3): 251.
55. Sanyahumbi D., Duncan J.R., Zhao M., van Hille R. Removal of lead from solution by the non-viable biomass of the water fern Azolla filiculoi. *Biotechnol. Lett*. 1998. **20**: 745.
56. Iqbal M., Saeed A., Zafar S.I. FTIR spectrophotometry, kinetics and adsorption isotherms modeling, ion exchange, and EDX analysis for uderstanding the mechanism of Cd^{2+} and Pb^{2+} removal by mango peel waste. *J. Hazard. Mater*. 2009. **164**(1): 161.
57. Pagnanelli F., Mainelli S., Vegliò F., Toro L. Heavy metal removal by olive pomace: biosorbent characterisation and equilibrium modelling. *Chem. Eng. Sci*. 2003. **58**(20): 4709.
58. Singh K.K., Talat M., Hasan S.H. Removal of lead from aqueous solutions by agricultural waste maize bran. *Bioresource Technol*. 2006. **97**(16): 2124.

59. Karnitz O., Gurgel L.V.A., De Melo J.C.P., Botaro V.R., Melo T.M.S., Gil L.F. Adsorption of heavy metal ion from aqueous single metal solution by chemically modified sugarcane bagasse. *Bioresource Technol*. 2007. **98**(6): 1291.
60. Kolomiiets Y.O., Palchik O.V., Dzyazko Yu.S., Yatsenko T.V., Ponomaryova L.M., Ogenko V.M. Sorbents based on biopolymers of different origin containing magnetite for removal of oil products and toxic ions from water. *Him. Fiz. Tehnol. Poverhni.* 2023. **14**(1): 121.
61. Noli F., Kapashi E., Kapnisti M. Biosorption of uranium and cadmium using sorbents based on Aloe vera wastes. *J. Environ. Chem. Eng*. 2019. **7**(2): 102985.
62. Sirry S.M., Aldakhil F., Alharbi O. M. L., Ali I. Chemically treated date stones for uranium (VI) uptake and extraction in aqueous solutions. *J. Mol. Liq*. 2019. **273**: 192.
63. Noli F., Kapashi E., Avgerinou A. Uranium and thorium retention onto sorbents from rawand modified pomegranate peel. *Water Air Soil Pollut.* 2021. **232**(10): 437.
64. Zhang X.T., Jiang D.M., Xiao Y.Q., Chen J.C., Hao S., Xia L.S. Adsorption of uranium (VI) from aqueous solution by modified rice stem. *J. Chem.* 2019. **2019**: 6409504.
65. Yi Z.J., Yao J., Chen H.L., Wang F., Yuan Z.M., Liu X. Uranium biosorption from aqueous solution onto Eichhornia crassipes. *J. Environ. Radioact.* 2016. **154**: 43.
66. Li X., Li F., Jin Y., Jiang C. The uptake of uranium by tea wastes investigated by batch, spectroscopic and modeling techniques. *J. Mol. Liq.* 2015. **209**: 413.
67. Bakather O.Y., Zouli N., Abutaleb A., Mahmoud M.A., Daher A., Hassan M., Eldoma M.A., Alasweda S.O., Fowad A.A. Uranium (VI) ions uptake from liquid wastes by Solanum incanum leaves: Biosorption, desorption and recovery. *Alexandria Eng. J.* 2020. **59**(3): 1495.
68. Šabanović E., Muhić-Šarac T., Nuhanović M., Memić M. Biosorption of uranium(VI) from aqueous solution by Citrus limon peels: kinetics, equlibrium and batch studies. *J. Radioanal. Nucl. Chem.* 2018. **319**(1): 425.
69. Smječanin N., Nuhanović M., Sulejmanović J. Study of uranium biosorption process in aqueous solution by red beet peel. *J. Radioanal. Nucl. Chem.* 2022. **331**: 1459.
70. Nuhanović M., Grebo M., Draganović S., Memić M., Smječanin N. Uranium (VI) biosorption by sugarbeet pulp: equilibrium, kinetic and thermodynamic studies. *J. Radioanal. Nucl. Chem.* 2019. **322**(3): 2065.
71. Ghandoor H., Zidan H., Mostafa, Khalil M., Ismail M. Synthesis and some physical properties of magnetite (Fe_3O_4) nanoparticles. *Int. J. Electrochem. Sci*. 2012. **7**(6): 5734.
72. Saavedra-Labastida E., Díaz-Nava M.C., Illescas J. Comparison of the removal of an anionic dye from aqueous solutions by adsorption with organically modified clays and their composites. *Water Air Soil Pollut*. 2019. **230**: 88.
73. Kadam B.V., Maiti B., Sathe R.M. Selective spectrophotometric method for the determination of uranium(VI). *Analyst*. 1981. **106**(1263): 724.
74. Kenney J.P.L., Kirby M.E., Cuadros J., Weiss D.J. A conceptual model to predict uranium removal from aqueous solutions in water–rock systems associated with low- and intermediate-level radioactive waste disposal. *RSC Adv*. 2017. **7**(13): 7876.
75. Ho Y.S., McKay G. Pseudo-second order model for sorption processes. *Process Biochem.* 1999. **34**(5): 451.
76. Largitte L., Pasquier R. A review of the kinetics adsorption models and their application to the adsorption of lead by an activated carbon. *Chem. Eng. Res. Des.* 2016. **109**: 495.
77. Al-Ghouti M.A., Da'ana D.A. Guidelines for the use and interpretation of adsorption isotherm models: A review. *J. Hazard. Mater*. 3030. **393**: 122383.
78. Dzyazko Yu.S., Rozhdestvenska L.M., Kudelko K.O., Fedina I.V., Ponomaryova L.M., Nikovska G.M., Dzyazko O.G. Hydrated iron oxide embedded to natural zeolite: effect of nanoparticles and microparticles on sorption properties of composites. *Water Air Soil Pollut.* 2022. **233**(6): 205.

Received 22.07.2024, accepted 25.11.2024